Diffusion Directions Imaging (DDI)

Aymeric Stamm, Patrick Pérez, Christian Barillot

INSTITUT NATIONAL DE RECHERCHE EN INFORMATIQUE ET EN AUTOMATIQUE

Diffusion Directions Imaging (DDI)

Aymeric Stamm* — Patrick Pérez† — Christian Barillot*

N° 7683

July 2011

Computational Medicine and Neurosciences

ISSN 0249-6399 ISRN INRIA/RR--7683--FR+ENG

INSTITUT NATIONAL
DE RECHERCHE
EN INFORMATIQUE
ET EN AUTOMATIQUE

INRIA

centre de recherche
RENNES - BRETAGNE ATLANTIQUE

Diffusion Directions Imaging (DDI)

Aymeric Stamm* , Patrick Pérez† , Christian Barillot*

Theme : Computational Medicine and Neurosciences
Computational Sciences for Biology, Medicine and the Environment
Équipe-Projet *VisAGeS
†Technicolor Research & Innovation

Rapport de recherche n° 7683 — July 2011 — 26 pages

Abstract: Diffusion weighted magnetic resonance (DW-MR) imaging is the reference in vivo modality to study the connectivity of brain white matter. Several models have been proposed to process DW-MR signal. They include popular diffusion tensor imaging (DTI) as well as higher-order models (qballs, ODF). These approaches suffer from important drawbacks. Standard DTI is insufficiently robust to noise and cannot directly cope with multiple fiber directions. Higher-order approaches can alleviate these limitations but at the cost of increased acquisition time. In this research report we propose a new diffusion model, coined Diffusion Directions Imaging (DDI) to overcome these limitations. It is based on the direct modeling of the displacement of water molecules under directional diffusion as a sum of two random variables: a tri-dimensional Gaussian vector and a two-dimensional von Mises-Fisher one, the latter capturing the directional statistics. We derive a closed form expression for the corresponding pdf and consider mixtures of such pdfs to handle multiple fiber directions. Under this model, we then derive a closed form expression of DW-MR measurements and exploit it to estimate diffusion parameters from noisy signals. On synthetic data, this new model proves more accurate and more robust to noise than DTI or ODF for estimating fiber directions. We also demonstrate its ability to handle multiple diffusion directions with a limited number of acquisitions. Finally, we show its good behaviour on real data with both isotropic and anisotropic regions.

Key-words: diffusion magnetic resonance imaging, imaging biomarkers, von Mises & Fisher distribution, brain white matter modeling

Centre de recherche INRIA Rennes – Bretagne Atlantique
IRISA, Campus universitaire de Beaulieu, 35042 Rennes Cedex
Téléphone : +33 2 99 84 71 00 — Télécopie : +33 2 99 84 71 71

Diffusion Directions Imaging (DDI)

Résumé : L'imagerie par résonance magnétique pondérée en diffusion (DW-MRI) est la modalité *in vivo* de référence pour étudier les connectivités neuronales dans la matière blanche du cerveau. Plusieurs modèles ont été proposés pour traiter les données issues de ce type d'imagerie. Le plus répandu est connu sous le nom de Diffusion Tensor Imaging (DTI) et, récemment, des modèles d'ordre supérieur (qballs, ODF) ont été introduits. Ces approches présentent des inconvénients importants. Le modèle standard DTI est insuffisamment robuste au bruit et ne permet pas d'estimer des croisements (ou bifurcations) de fibres. Les approches d'ordre supérieur peuvent atténuer ces limites, mais au prix d'un temps d'acquisition augmenté. Dans ce rapport de recherche nous proposons un nouveau modèle de diffusion, intitulé Diffusion Directions Imaging (DDI) qui permet de surmonter ces limitations. Il est basé sur la modélisation directe du déplacement aléatoire des molécules d'eau comme une somme de deux variables aléatoires: un vecteur tri-dimensionnel suivant une loi Gaussienne et un vecteur bi-dimensionel suivant une loi de von Mises-Fisher. Nous en dérivons l'expression de la pdf correspondante et proposons un mélanges de ces pdfs pour permettre l'estimation de plusieurs directions de fibre. Sous les hypothèses de ce modèle, nous avons ensuite dériver une expression analytique de l'intensité du signal de diffusion et nous l'exploitons pour estimer les paramètres de notre modèle DDI Ã partir des signaux bruités. Sur des données synthétiques, ce nouveau modèle s'avère plus précis et plus robuste au bruit que le DTI ou ODF pour estimer les directions de fibre. Nous avons également démontrer sa capacité Ã détecter de multiples directions de fibre avec un nombre limité d'acquisitions. Enfin, nous montrons son bon comportement sur des données réelles avec des régions à la fois isotrope et anisotrope.

Mots-clés : diffusion magnetic resonance imaging, biomarqueurs d'imagerie, distribution de von Mises & Fisher, modélisation de la matière blanche cérébrale

Contents

1 Introduction and Motivations

Diffusion magnetic resonance imaging (dMRI) [1] allows *in-vivo* and non-invasive investigation of biological tissue structure. A widespread application of dMRI is the study and analysis of the brain white matter constituted of intricate fiber bundles (axons) into which the diffusion is restricted and allows to infer their geometry (orientations, diameter, etc).

Standard dMRI sequences often boil down to *q-space imaging* [2] in which, in practice, a series of magnetic field gradients $\boldsymbol{q}$ is applied to a subject's brain. It makes the assumption that the width δ of these gradients is very short and negligible with respect to (wrt) the diffusion time Δ between two successive applied gradients. Under this assumption, the magnetic field gradients $\boldsymbol{q}$ are not time-dependent anymore: their directions are thus directly encoded and their intensities are encoded via the so-called b-value according to [2] $b = \tau\|\boldsymbol{q}\|^2$, where $\tau := \Delta - \delta/3$ is the approximate diffusion time.

For each magnetic field gradient, the **raw diffusion signal** is the intensity (modulus) of the complex magnetization of all contributing spins [3] corrupted by measurement noise which, in the literature, is assumed to follow either a Rice probability distribution [4] or a non-central χ^2 probability distribution in case of parallel imaging [5]. Under the q-space imaging formalism, the following relation holds [6, 7]:

$$\frac{A^\star(\boldsymbol{q})}{A^\star(\boldsymbol{0})} = \int_{\mathbb{R}^3} f_{\mathbf{x}}(\boldsymbol{x}) \mathrm{e}^{i\boldsymbol{q}'\boldsymbol{x}} \mathrm{d}\boldsymbol{x} \ , \tag{1}$$

where $A^\star(\boldsymbol{q})$ is the theoretical complex magnetization at diffusion time τ when a magnetic field gradient $\boldsymbol{q}$ is applied, $A^\star(\mathbf{0})$ is the complex magnetization in absence of magnetic field gradient, $\mathbf{x}$ is the 3-dimensional random displacement of the water molecules and $f_{\mathbf{x}}$ is termed the **diffusion probability density function** (pdf). Inferring the micro-structure of the tissues requires to reconstruct the diffusion pdf from raw diffusion signals $S(\boldsymbol{q})$ which, in absence of measurement noise, read $A(\boldsymbol{q}) = |A^\star(\boldsymbol{q})|$ (**theoretical diffusion signals**). Methods for the reconstruction of the diffusion pdf have thus been devised to estimate some of its features from the raw diffusion signals [8] and hinge on four major q-space sampling schemes:

Full Sampling. If the q-space is entirely sampled on a Cartesian lattice with sufficient density (so that accurate fast Fourier transform (FFT) can be performed), model-free Diffusion Spectrum Imaging (DSI) method [9] proposes an accurate reconstruction of the symmetric part of the diffusion pdf, termed the ensemble average propagator (EAP) [10]. Assuming the diffusion pdf to be symmetric implies that the normalized theoretical complex magnetization (left part of Eq.(**??**)) is equal to its modulus, the Fourier transform (FT) of which directly yields the EAP. An estimation of the EAP is thus obtained by FFT of the normalized raw diffusion signals. A full sampling of the q-space however requires a huge number of both encoding b-values including high b-values (upwards of 8000s/mm^2) and encoding directions (upwards of 500) leading to an acquisition time of several hours [11].

Multi-Shell Imaging (MSI) Sampling. MSI consists in sampling the q-space over a large number of encoding directions (upwards of 60) uniformly spread on **several** spheres (usually 2-4 b-values, both low and high). Even if it significantly reduces the acquisition time wrt to a full sampling, it takes upwards of 30 min. This spherical sampling is however not suited to DSI. Adjusting the raw diffusion signal to a Cartesian lattice by means of bilinear interpolation yields Hybrid Diffusion Imaging (HYDI) [12]. Other model-free methods based on MSI sampling provide estimates of the EAP by expanding the raw diffusion signals by means of (i) 4-th order tensors [13, 14], (ii) the spherical polar Fourier basis up to a given order [15, 16] or (iii) the solid harmonics basis up to a given order giving its name to Diffusion Propagator Imaging (DPI) [17]. An MSI-based method for the reconstruction of the full diffusion pdf (including symmetric and asymmetric dislacements) is also proposed in [18], using the Gram-Charlier expansion of the raw diffusion signal up to a given order. Alternatively, model-dependent methods that assumes the diffusion pdf to be a mixture of Gaussian densities (e.g. the "multi-Gaussian" model [19], the "multi-Watson" model [20], and the Ball & Stick model [21]) make use of MSI [22] and provide a parametric estimation of the EAP.

High Angular Resolution Diffusion Imaging (HARDI) Sampling. HARDI consists in sampling the q-space over a large number of encoding directions (upwards of 60) uniformly spread on a high-radius **single** sphere (single high b-value, typically greater than 1500s/mm^2) [23] which further reduces the acquisition time wrt MSI (lower bound of about 15 min). Model-free methods for the reconstruction of the diffusion pdf using HARDI sampling mainly revolve around q-ball imaging (QBI) [24] and diffusion orientation transform (DOT) [25]. Both methods focus on the estimation of a specific angular feature of the EAP, namely the diffusion orientation distribution function (dODF) (to be precise, an approximation thereof) defined as the density of the marginal prob-

ability distribution of the molecular displacements on the 2-dimensional unit sphere [26] and the isoradius of the EAP, respectively. QBI originally estimates the dODF by expanding the raw diffusion signals by means of a spherical radial basis function with Gaussian kernel [24] but further works exhibit a faster and more robust QBI by expanding the raw diffusion signals by means of the spherical harmonics (SH) basis [27, 28, 29]. As for DOT, the isoradius of the EAP is estimated by expanding the Fourier-Bessel transform of the raw diffusion signals by means of the SH basis [25]. Model-dependent methods for the reconstruction of the diffusion pdf using HARDI sampling are (i) the composite hindered and restricted mixture model, coined CHARMED [30], of which one component is an isotropic Gaussian density and the others are Neuman-type densities for restricted diffusion within a cylinder [31] and (ii) spherical deconvolution models [32, 33] which estimate the fiber orientation distribution function (fODF). The latter methods assume that the raw diffusion signals are the result of the convolution between the fODF and a kernel reflecting the diffusion within a given fiber. This kernel is in turn assumed (i) of Gaussian-type [34, 27, 35], (ii) of Rigaut-type [36] or (iii) sinusoidal [37] (which is an alternative formulation of persistent angular structure MRI (PAS-MRI) [38]). Data-dependent kernels are also proposed in [39, 40, 41].

Low Angular Resolution Diffusion Imaging (LARDI) Sampling. LARDI consists in sampling the q-space over a low number of encoding directions (typically less than 30) uniformly spread on a low-radius **single** sphere (single low b-value, typically lower than 1500s/mm^2) so that the acquisition time drops below 10 min. To the best of our knowledge, the only method for the reconstruction of the diffusion pdf to date compatible with LARDI is diffusion tensor imaging (DTI) [42]. It is a model-dependent method that provides a parametric estimation of the EAP by assuming the latter to be a 3-dimensional centered Gaussian pdf parametrized by a *diffusion tensor*. The derivation of Eq.(**??**) is then straightforward and thus the raw diffusion signal can be analytically expressed as a function of the diffusion tensor. Unlike all the other methods, the major drawback of the DTI method (apart from the fact that it implies symmetry of the molecular displacements) is that it does not account for intra-voxel white matter fiber heterogeneity brought to light in [19].

Clinical protocols often include, in addition to the dMRI sequence, other types of sequences (e.g. 3D T1, FLAIR and T2 for vascular pathologies, perfusion, resting-state, magnetization transfer, etc). Neurologists thus tally with an upper bound of 10 min for the acquisition time (AT) of the dMRI sequence so that the whole protocol does not exceed half an hour. Even if the recent ongoing research proposes significant reduction of the acquisition time for full sampling or MSI sampling notably by means of compressed sensing [43, 44], they are up to now still prohibitively time-consuming (upwards of 20 min). In a clinical setting, only dMRI data sets acquired with LARDI sampling of the q-space can thus be used to infer the diffusion pdf. In addition, because of the intra-voxel white matter fiber heterogeneity, the method for the reconstruction of the diffusion pdf shall account for multiple fiber directions. Table 1 shows that there is no state-of-the-art method for the reconstruction of the diffusion pdf that both relies on LARDI sampling of the q-space and allows to estimate several fiber directions.

Table 1: Summary of the different sampling schemes of the q-space, with associated lower bound of the acquisition time and indication on whether associated state-of-the-art methods for the reconstruction of the diffusion pdf allow to estimate multiple fiber directions or not.

Sampling	AT Lower bound	Multi-fiber
Full	30 min	yes
MSI	20 min	yes
HARDI	15 min	yes
LARDI	10 min	no

The contribution of this work is to propose a new method for the reconstruction of the diffusion pdf, coined diffusion directions imaging (DDI), that fulfills the following four objectives:

1. Being compatible with dMRI data sets acquired in **maximum 10 min**.
2. Estimating **multiple fiber directions**.
3. Allowing for the **retrospective analysis of DTI repositories** acquired in the past.
4. Accounting for both **symmetric and asymmetric molecular displacements**.

We introduce the new proposed method in Section 2. Then, we evaluate its robustness to Rician noise, we validate the method on simulated dMRI data sets and we show its applicability and performances on clinical dMRI data sets in Section 3. Finally, we propose a discussion on both the theoretical and practical aspects of the method in Section 4.

2 Methods

In a given voxel, the diffusion process induces, after a diffusion time τ, a random displacement $\delta\mathbf{x}$ of the water molecules, the pdf of which is the **diffusion pdf**. The simplest and most widespread method for the reconstruction of the diffusion pdf, which is to date the only method through which clinicians analyze dMRI data sets, is the model-dependent DTI method [42]. It assumes that $\delta\mathbf{x} = \sqrt{2\tau}\mathbf{w}$, where $\mathbf{w}$ follows a 3-dimensional centered Gaussian probability distribution whose covariance matrix D is termed the *diffusion tensor*. Because of the nature of the Gaussian probability distribution, (i) it assumes a unique direction of diffusion per voxel, (ii) it mixes up the angular and radial component of the diffusion and (iii) it only models the symmetric molecular displacements, discarding the asymmetric ones, which thereby only allows for the reconstruction of the EAP.

Nevertheless, model-dependent methods seem to be the key to reconstructing the diffusion pdf from clinically acquired data sets. Therefore, we propose an alternative parametric probability distribution for the random variable $\mathbf{w}$ to remedy the weaknesses in the DTI method. The random motion of water molecules in the white matter depends on the surrounding tissue structure. Because of the intra-voxel white matter fiber heterogeneity, first brought to light in [19], we assume that, in each voxel, water molecules can be divided into several compartments.

First, we describe how we model the diffusion within a single compartment and how we can easily obtain some diffusion features of particular interest (e.g. direction of diffusion, associated measure of anisotropy and radial displacement). Then, we introduce our multi-compartment model of the diffusion pdf, coined Diffusion Directions Imaging (DDI), of which we propose a motivated parametrization. Second, we depict how we estimate the parameters of the DDI model from the raw diffusion signals. In particular, (i) we establish the analytical relation between the theoretical diffusion signals and the parameters of the DDI model, (ii) we go into details regarding some interesting asymptotic behaviors of this analytical relation and (iii) we explain how we handle both the inherent measurement noise (which the raw diffusion signals are corrupted with) and the underlying model selection problem to improve the robustness of the estimation.

2.1 The new proposed diffusion model

In this subsection, we refer to the diffusion pdf as the pdf of the random variable $\mathbf{w}$ instead of the pdf of the molecular displacement $\delta\mathbf{x}$. This can be done without loss of generality since $\mathbf{x}$ is equal to $\delta\mathbf{x}$ up to the multiplicative scalar factor $\sqrt{2\tau}$, which only depends on the diffusion time.

2.1.1 Single-compartment model

Local diffusion modeling. Within each compartment, the random 3-dimensional displacement of water molecules is the combination of a random 2-dimensional direction and a random 1-dimensional displacement along that direction. In the single-compartment model, we thus focus on (i) better separating these angular and radial components of the diffusion and (ii) integrating a possible asymmetry in the model.
Ideally, one could think of expressing the random variable $\mathbf{w}$ in spherical coordinates as $\mathbf{w} = r\mathbf{v}$ so that both the radial component (r) and the angular component ($\mathbf{v}$) could be completely modeled apart. However, to the best of our knowledge, there is no pair of known parametric probability distributions (a univariate one and a directional one to model r and $\mathbf{v}$ respectively) that leads to an analytical relation between the theoretical diffusion signals and the parameters of the subsequent model, making any such models pointless in conjunction with dMRI data sets.
Aware of this intricate mathematical issue, we express the random variable $\mathbf{w}$ as the sum of two independent random variables, which is convenient for the analytical derivation of Eq.(1). In essence, we assume that $\mathbf{w} = \mathbf{v} + \mathbf{z}$, where:
• $\mathbf{v}$ follows a **von Mises & Fisher** probability distribution (see Appendix B) defined on the 2-dimensional sphere of radius $R > 0$ and parametrized by its mean direction $\boldsymbol{\mu}$, with $\|\boldsymbol{\mu}\| = 1$, and its concentration parameter $\kappa \geq 0$. The higher the concentration parameter, the more likely the water molecules are to diffuse along $\boldsymbol{\mu}$; when it is nil, the direction of molecular displacements is uniformly distributed over the sphere; $\boldsymbol{\mu}$ can thus be interpreted as the direction of the fibers which constrain the diffusion, whereas κ can be interpreted as a measure of anisotropy of the diffusion. The von Mises & Fisher probability distribution admits a pdf on the 2-dimensional sphere of radius R. Its expression is given in [45] for $R = 1$ and can easily be extended on the sphere of radius

$R > 0$ by affine transformation. For any $\boldsymbol{v} \in \mathbb{R}^3$ such that $\|\boldsymbol{v}\| = R$, we indeed have:

$$f_{\mathbf{v}}(\boldsymbol{v}; \boldsymbol{\mu}, \kappa, R) = \frac{1}{R^3} \frac{\kappa}{4\pi \mathrm{sh}\, \kappa} \mathrm{e}^{\frac{\kappa}{R} \boldsymbol{\mu}' \boldsymbol{v}} \ . \tag{2}$$

• $\mathbf{z}$ follows a centered **Gaussian** probability distribution defined on $\mathbb{R}^3$ and parametrized by a cylindrically constrained covariance matrix D, akin to the diffusion tensor in the constrained DTI model proposed in [46], completely determined by its condition number (i.e. the ratio of its largest non-zero eigenvalue to its smallest non-zero eigenvalue) set to $\kappa + 1$ and its largest eigenvalue set to R^2 with associated eigenvector set to $\boldsymbol{\mu}$ so that $D = \dfrac{R^2}{\kappa + 1} (I_3 + \kappa \boldsymbol{\mu} \boldsymbol{\mu}')$, where I_3 is the 3×3 identity matrix. If $\kappa \to +\infty$, then $D = R^2 \boldsymbol{\mu} \boldsymbol{\mu}'$ and thus R represents the radial displacement along the fiber direction $\boldsymbol{\mu}$; if $\kappa \to 0$, then $D = R^2 I_3$ and thus R represents the radial displacement along any direction. The centered "cylindrical" Gaussian pdf can be elegantly expressed using the Sherman-Morrison Woodbury identity [47] to invert D. For any $\boldsymbol{z} \in \mathbb{R}^3$, we indeed have:

$$f_{\mathbf{z}}(\boldsymbol{z}; \boldsymbol{\mu}, \kappa, R) = \frac{\kappa + 1}{\left(R\sqrt{2\pi}\right)^3} \mathrm{e}^{-\frac{(\kappa+1)\|\boldsymbol{z}\|^2 - \kappa(\boldsymbol{\mu}'\boldsymbol{z})^2}{2R^2}} \ . \tag{3}$$

• $\mathbf{v}$ and $\mathbf{z}$ are statistically independent.

The diffusion pdf is thereby obtained by a non trivial convolution of the von Mises & Fisher pdf defined on the 2-dimensional sphere of radius R according to Eq.(2) and the Gaussian pdf defined on $\mathbb{R}^3$ according to Eq.(3), and is parametrized by $\boldsymbol{\mu}$ (unit vector), $\kappa \geq 0$ and $R > 0$ (i.e. four parameters). For any $\boldsymbol{w} \in \mathbb{R}^3$, we have (see Appendix C):

$$\begin{aligned} f_{\mathbf{w}}(\boldsymbol{w}; \boldsymbol{\mu}, \kappa, R) &= c(\kappa, R) \mathrm{e}^{-\frac{1}{2}\left((\kappa+1)w_\perp^2 + w_{/\!/}^2\right)} \\ &\times \int_{-1}^{1} \mathrm{e}^{\frac{\kappa}{2}t^2 + (\kappa + w_{/\!/})t} I_0\left((\kappa+1) w_\perp \sqrt{1-t^2}\right) dt \ , \end{aligned} \tag{4}$$

where (i) $(w_{/\!/}, w_\perp) := R^{-1}\left(\boldsymbol{\mu}'\boldsymbol{w}, \sqrt{\|\boldsymbol{w}\|^2 - (\boldsymbol{\mu}'\boldsymbol{w})^2}\right)$,

(ii) $c(\kappa, R) := \dfrac{\kappa(\kappa+1)\sqrt{2}}{8\pi^{3/2} R^3 \mathrm{sh}\,(\kappa)} \mathrm{e}^{-\frac{\kappa+1}{2}}$ and (iii) I_0 is the zero-*th* order modified Bessel function [48], with the convention that $\boldsymbol{\mu}'\boldsymbol{w} = \|\boldsymbol{w}\|$ for any $\boldsymbol{w} \in \mathbb{R}^3$ when $\kappa = 0$.

Diffusion features. The random variable $\mathbf{v}$ models exclusively the angular component of the diffusion while the random variable $\mathbf{z}$ mainly models the radial component of the diffusion. Indeed, the shape of the covariance matrix D of the Gaussian probability distribution, with its two smallest eigenvalues being equal, is analogous to a cylinder whose axis lies along the mean direction $\boldsymbol{\mu}$ of the von Mises & Fisher probability distribution. This prevents water molecules from strongly deviating from the direction $\boldsymbol{\mu}$, which makes the largest eigenvalue R^2 of D being a fair approximation of the squared radial displacement.

Within each compartment of each voxel, the **putative fiber direction** is thereby a natural output ($\boldsymbol{\mu}$) of this single-compartment model as well as the **radial displacement of water molecules** (R) along this direction. The κ parameter completes the description of the diffusion in a compartment by assessing the degree of local anisotropy.

The covariance matrix D involved in our single-compartment model is akin to a diffusion tensor. Its largest and smallest eigenvalues, R^2 and $R^2/(\kappa+1)$ respectively, can thus be interpreted as the **principal and transverse diffusivities**, respectively.
For ease of interpretation by clinicians, we can additionally relate κ and R to the **fractional anisotropy** (FA) and the **mean diffusivity** (MD) [49]. After some trivial calculations, we indeed obtain:

$$\mathrm{FA} = \frac{\kappa}{\sqrt{(\kappa+1)^2+2}} , \qquad \text{for any } \kappa \geq 0 , \tag{5}$$

$$\mathrm{MD} = \left(1+\frac{\kappa}{3}\right)\frac{R^2}{\kappa+1} , \qquad \text{for any } \kappa \geq 0 ,\ R > 0 .$$

2.1.2 Multi-compartment Model

Mixture model. Due to the low number of parameters of our single-compartment model (4), we can embody it within a multi-compartment model, which can account for more than one fiber direction within each voxel with still a low number of parameters. This approach was pioneered in [19, 21], using DTI as single-compartment model, and was quite promising. Unfortunately, this model, a.k.a. "multi-tensor" model, requires dMRI data sets acquired on multiple spherical shells [22], which is not compatible with clinical settings. We thereby propose the same approach using our single-compartment model instead.
Assuming m different fiber directions within a given voxel, we model the diffusion pdf as a mixture of m pdfs (**fiber compartments**) having the common parametric form given in Eq.(4) with parameters $\{\boldsymbol{\mu}_i, \kappa_i, R_i\}_{i\in[\![1,m]\!]}$. We also include an additional pdf in the mixture to account for isotropic diffusion (**isotropic compartment**). This pdf follows the general form given in Eq.(4) with $\kappa = 0$: in that case, for any $\boldsymbol{w} \in \mathbb{R}^3$, defining $w_R = \|\boldsymbol{w}\|/R$, one can show that:

$$f_{\mathrm{iso}}(\boldsymbol{w}; R) = 2c(0,R)\mathrm{e}^{-\frac{w_R^2}{2}}\frac{\mathrm{sh}\, w_R}{w_R} . \tag{6}$$

Mixture weights. We have to associate a mixture weight to each of the $m+1$ pdfs that compose the mixture. Let us begin with the weight of the *i-th* fiber compartment, $i \in [\![1,m]\!]$.
• Case $\mathrm{FA}_i = 0$: The *i-th* fiber compartment contains water molecules diffusing along directions that are not regrouped around the direction $\boldsymbol{\mu}_i$ at all, making $\boldsymbol{\mu}_i$ being a **fictitious** fiber direction. It must thereby have a null mixture weight.
• Case $\mathrm{FA}_i = 1$: the *i-th* fiber compartment contains water molecules diffusing strictly along direction $\boldsymbol{\mu}_i$, making $\boldsymbol{\mu}_i$ being a **true** fiber direction. It must thereby have the maximum possible mixture weight.
• Case $0 < \mathrm{FA}_i < 1$: the *i-th* fiber compartment contains water molecules diffusing along directions that are regrouped around the direction $\boldsymbol{\mu}_i$ with a concentration proportional to FA_i, making $\boldsymbol{\mu}_i$ being a **putative** fiber direction with "degree of belief" proportional to FA_i. It must thereby have a mixture weight proportional to FA_i.
Assuming that fiber compartments associated to true fiber directions have equal mixture weights leads to a value of $1/m$ for such weights. To account for all the previous requirements, we thereby set the weight of the *i-th* fiber compartment

to FA_i/m, $i \in [\![1,m]\!]$. The weight of the isotropic compartment consequently reads $1 - \sum_{i=1}^{m} \mathrm{FA}_i/m$.

Mixture diffusivities. Based on the argument that nerve fibers share similar dimensions, the principal and transverse diffusivities are often assumed identical in each compartment [50, 40]. We follow the same lines for the transverse diffusivity but we choose to let each compartment have its own principal diffusivity to strengthen the estimation of the associated direction which is a putative fiber direction. For any $i \in [\![1,m]\!]$, we thus have $R_i^2 = (\kappa_i + 1)\lambda$, where $\lambda > 0$ is the **common** transverse diffusivity.

The DDI model. Our assumptions on the form of the diffusion pdf (mixture model section) along with the assumptions relative to its parametrization (mixture weights and mixture diffusivities sections) allows us to state our DDI model.
Assuming m putative fiber directions in the voxel, DDI proposes to model the diffusion pdf as follows:

$$\begin{aligned} & f_{\mathbf{w}}\left(\boldsymbol{w}; \{\boldsymbol{\mu}_i, \kappa_i\}_{i\in[\![1,m]\!]}, \lambda\right) \\ &= \left(1 - \frac{1}{m}\sum_{i=1}^{m} \mathrm{FA}(\kappa_i)\right) f_{\mathrm{iso}}\left(\boldsymbol{w}; \sqrt{\lambda}\right) \\ &+ \frac{1}{m}\sum_{i=1}^{m} \mathrm{FA}(\kappa_i) f_i\left(\boldsymbol{w}; \boldsymbol{\mu}_i, \kappa_i, \sqrt{(\kappa_i+1)\lambda}\right) \ , \end{aligned} \tag{7}$$

where FA is given by Eq.(5), f_{iso} is given by Eq.(6) and f_i is given by Eq.(4), for any $i \in [\![1,m]\!]$.
It is thus parametrized by $3m+1$ parameters (e.g. 1 parameter for the isotropic DDI model, 4 parameters for the 1-fiber DDI model, 7 parameters for the 2-fiber DDI model, and so on), namely:
- the spherical coordinates $(\theta_i, \phi_i) \in [0,\pi] \times [0, 2\pi[$ of the putative fiber direction $\boldsymbol{\mu}_i$, for any $i \in [\![1,m]\!]$;
- the concentration of water molecules $\kappa_i \geq 0$ around the putative fiber direction $\boldsymbol{\mu}_i$, for any $i \in [\![1,m]\!]$;
- the transverse diffusivity $\lambda > 0$, common to all compartments.

2.2 Estimation of the DDI Parameters

2.2.1 Analytical expression of the theoretical diffusion signal

An analytical relation between the theoretical diffusion signal $A(b, \boldsymbol{g})$, which depends on the b-value and direction ($\boldsymbol{g}$) of the applied magnetic field gradient, and the parameters of the DDI model can be derived by computing analytically the integral in Eq.(1).

This integral is, by definition, the characteristic function (cf) of the real 3-dimensional random variable $\delta\mathbf{x} = \sqrt{2\tau}\mathbf{w}$, meaning that Eq.(1) can be written

(taking the modulus of each part of the equation):

$$\begin{aligned}\frac{A(b,\boldsymbol{g})}{A(\mathbf{0})} &= \left|\varphi_{\delta\mathbf{x}}\left(\sqrt{\frac{b}{\tau}}\boldsymbol{g}\right)\right| \\ &= \left|\varphi_{\sqrt{2\tau}\mathbf{w}}\left(\sqrt{\frac{b}{\tau}}\boldsymbol{g}\right)\right| = \left|\varphi_{\mathbf{w}}\left(\sqrt{2b}\boldsymbol{g}\right)\right| \ .\end{aligned} \tag{8}$$

Assuming that $\mathbf{w}$ follows the DDI model, i.e. that its pdf is given by Eq.(7), $\varphi_{\mathbf{w}}\left(\sqrt{2b}\boldsymbol{g}\right)$ reads:

$$\begin{aligned}&\varphi_{\mathbf{w}}\left(\sqrt{2b}\boldsymbol{g};\{\boldsymbol{\mu}_i,\kappa_i\}_{i\in[\![1,m]\!]},\lambda\right) \\ &= \left(1-\frac{1}{m}\sum_{i=1}^{m}\mathrm{FA}_i\right)\varphi_{\mathrm{iso}}\left(\sqrt{2b}\boldsymbol{g};\sqrt{\lambda}\right) \\ &+\frac{1}{m}\sum_{i=1}^{m}\mathrm{FA}_i\,\varphi_i\left(\sqrt{2b}\boldsymbol{g};\boldsymbol{\mu}_i,\kappa_i,\sqrt{(\kappa_i+1)\lambda}\right) \ ,\end{aligned} \tag{9}$$

where FA_i is given by Eq.(5) with $\kappa=\kappa_i$, $\forall i\in[\![1,m]\!]$,

$$\varphi_{\mathrm{iso}}\left(\sqrt{2b}\boldsymbol{g};\sqrt{\lambda}\right) = \mathrm{e}^{-b\lambda}\frac{\sin\sqrt{2b\lambda}}{\sqrt{2b\lambda}} \ , \text{ and}$$

$$\begin{aligned}\varphi_i\left(\sqrt{2b}\boldsymbol{g};\boldsymbol{\mu}_i,\kappa_i,\sqrt{(\kappa_i+1)\lambda}\right) &= \mathrm{e}^{-b\lambda\left(1+\kappa_i(\boldsymbol{\mu}_i'\boldsymbol{g})^2\right)} \\ \times\frac{\kappa_i}{\mathrm{sh}\,\kappa_i}&\begin{cases}\dfrac{\sin\sqrt{2(\kappa_i+1)b\lambda-\kappa_i^2}}{\sqrt{2(\kappa_i+1)b\lambda-\kappa_i^2}} \ , & \sqrt{2b}\boldsymbol{g}\in\Omega_i \ , \\ \dfrac{\mathrm{sh}\ (\alpha_i+i\beta_i)}{\alpha_i+i\beta_i} \ , & \sqrt{2b}\boldsymbol{g}\notin\Omega_i \ ,\end{cases}\end{aligned}$$

where Ω_i is defined in Eq.(14) replacing R_i with $\sqrt{(\kappa_i+1)\lambda}$ and $\alpha_i=\alpha_i\left(\sqrt{2b}\boldsymbol{g};\boldsymbol{\mu}_i,\kappa_i,\sqrt{(\kappa_i+1)\lambda}\right)$ and $\beta_i=\beta_i\left(\sqrt{2b}\boldsymbol{g};\boldsymbol{\mu}_i,\kappa_i,\sqrt{(\kappa_i+1)\lambda}\right)$ are given by Eq.(13), for any $i\in[\![1,m]\!]$.

Inserting Eq.(9) into Eq.(8) yields the analytical relationship between the theoretical diffusion signal $A(b,\boldsymbol{g})$ and the parameters $\left\{\{\boldsymbol{\mu}_i,\kappa_i\}_{i\in[\![1,m]\!]},\lambda\right\}$ of the DDI model.

2.2.2 Asymptotic behaviors

Two limiting cases of Eq.(8) and Eq.(9) need further investigations:

- Case $\kappa_i\to 0$, $\forall i\in[\![1,m]\!]$: it is the isotropic DDI model; all the FA are equal to 0 in the fiber compartments, the weights of which become nil; in that case, one can easily show that the theoretical diffusion signal does not depend on the encoding direction but only on the encoding b-value and reads:

$$A_{\mathrm{iso}}^{\mathrm{DDI}}(b;\lambda) = A(0)\mathrm{e}^{-b\lambda}\frac{\left|\sin\sqrt{2b\lambda}\right|}{\sqrt{2b\lambda}} \ ,$$

which is equal, up to a multiplicative factor, to the expression obtained using the isotropic DTI model [51]: $A_{\mathrm{iso}}^{\mathrm{DTI}}(b;\lambda)=A(0)\mathrm{e}^{-b\lambda}$. More precisely, when the

encoding b-value (or the diffusivity λ) is small, the isotropic DDI model behaves like the isotropic DTI model. When the encoding b-value (or the diffusivity λ) is large, the isotropic DDI model also behaves like the isotropic DTI model. These two situations, a.k.a. the *long wavelength limit* and *large displacement limit* respectively, have been carefully examined in [52] in which the same conclusions were reached. On the other hand, when the encoding b-value (or the diffusivity λ) is moderate (typically between 400 s/mm^2 and 3000 s/mm^2), we suggest a slight departure from the isotropic DTI model.

- Case $\kappa_i \to +\infty$, $0 < R_i^2 = (\kappa_i+1)\lambda < +\infty$, $\forall i \in [\![1,m]\!]$: it is the "perfectly anisotropic" DDI model; in each fiber compartment, the principal diffusivity R_i^2 is finite and the FA_i goes to 1 so that the isotropic mixing weight becomes nil; in that case, one can easily show that the theoretical diffusion signal reads:

$$A_\infty^{\mathrm{DDI}}\left(b,\boldsymbol{g};\{\boldsymbol{\mu}_i,R_i\}_{i\in[\![1,m]\!]}\right)=\frac{A(\mathbf{0})}{m}\sum_{i=1}^{m}\mathrm{e}^{-bR_i^2(\boldsymbol{\mu}_i'\boldsymbol{g})^2}$$

This limiting case of our DDI model is found to coincide with the model proposed in [20] using Watson distributions, which is a constrained multi-tensor model where the tensors have a unique non-zero eigenvalue and the compartments are equally weighted.

2.2.3 Estimation from noisy diffusion signals

Description of a dMRI data set. In its most general form, a dMRI data set is composed of $n_g \times n_b$ raw diffusion signals S_{jk}, $j \in [\![1,n_g]\!]$, $k \in [\![1,n_b]\!]$, acquired for n_g different encoding directions $\{\boldsymbol{g}_j\}_{j\in[\![1,n_g]\!]}$ and n_b different encoding b-values $\{b_k\}_{k\in[\![1,n_b]\!]}$. Each raw diffusion signal is corrupted by Rician noise [53, 4], as $S_{jk} \sim \mathrm{Rice}(A_{jk},\sigma_k)$, where $\sigma_k \geq 0$ is the standard deviation of the noise which depends on the b-value, and A_{jk} is the corresponding theoretical diffusion signal which is analytically related to the parameters of the DDI model.

Handling the Rician noise. Because of the Rician noise, in general, the mean of a raw diffusion signal S_{jk} does not match the corresponding theoretical diffusion signal A_{jk}. For moderate (typically greater than 3) signal-to-noise ratio (SNR), defined as $\mathrm{SNR}_{jk} = A_{jk}/\sigma_k$, the following Gaussian approximation of the Rician noise stands [4]: $S_{jk} \sim \mathrm{N}\left(\sqrt{A_{jk}^2+\sigma_k^2},\sigma_k^2\right)$. This approximation however requires (i) σ_k to be known which is not the case in practice and (ii) SNR_{jk} to be sufficiently high. These two issues are solved using the recursive linear minimum mean square error (RLMMSE) estimator for the Rician model introduced in [54].

Minimization problem. Assuming that the Gaussian approximation of the Rician noise stands, a least squares (LS) fitting is adequate. The estimation of the DDI parameters is indeed performed by minimizing the following criterion:

$$J\left(\{\boldsymbol{\mu}_i,\kappa_i\}_{i\in[\![1,m]\!]},\lambda;\{S_{jk}\}\right)= \tag{10}$$
$$\sum_{j=1}^{n_g}\sum_{k=1}^{n_b}\left(\frac{S_{jk}-\sqrt{A_{jk}^2\left(\{\boldsymbol{\mu}_i,\kappa_i\}_{i\in[\![1,m]\!]},\lambda\right)+\sigma_k^2}}{\sigma_k}\right)^2 .$$

The optimization of the cost function J is performed using the derivative-free new unconstrained optimization algorithm (NEWUOA) [55]. Each parameter of the DDI model is thus transformed into an unconstrained parameter using the general transformation $p = p_{\min} + p_{\max}\left(\sin(p^\star) + 1\right)/2$, where p is any parameter of the DDI model and $p^\star$ the associated unconstrained parameter. The value of $p_{\min}$ was set to 0 for all the parameters. The value of $p_{\max}$ was set to π for the parameters $\{\theta_i\}_{i\in[\![1,m]\!]}$, 2π for $\{\phi_i\}_{i\in[\![1,m]\!]}$, 30 for $\{\kappa_i\}_{i\in[\![1,m]\!]}$ and 0.005 for λ.

2.2.4 Model Selection

The DDI model also requires a model selection step since the number m of fiber directions in a voxel is not a priori known. In practice:

- We choose a maximum M of possible fiber directions within a voxel.
- We perform the estimation of the DDI parameters for $m \in \{0, 1, 2, \ldots, M\}$.
- We select the model with minimum corrected Akaike's Information Criterion (AICc) [56]:

$$\mathrm{AICc}(m) = \chi^2 + 6m + 2 + \frac{(6m+2)(3m+2)}{n-3m-2}\ ,$$

where χ^2 is the minimum value of the cost function J. In essence, this criterion is a modified version of the original AIC which accounts for the over-fitting problem that occurs when the AIC is computed from data sets with a too small sample size n.

3 Results

3.1 Experimental setup

Proposed model has been validated on both synthetic and clinical data. Simulations first allowed us to assess its robustness to noise and to draw comparisons with respect to the standard cylindrical-shaped DTI model and to an ODF-based method, namely Tensor-ODF [41]. Latter approach, whose implementation is available on-line, is one of the most recent and accurate ODF models. It is, in particular and in contrast with classical ODF-based methods, almost insensitive to the number of acquisition directions.

With the aim to focus on DDI ability to estimate fiber direction(s), we generated:

- Two datasets, R1 and R2, sampled from DDI model with $\kappa = 12.08$ and $\lambda = 2.1 \times 10^{-3}$ mm^2.s^{-1}. In R1, we consider a single fiber direction $\boldsymbol{\mu}_1 = (1/2, \sqrt{3}/2, 0)'$, whereas two crossing fiber directions $\boldsymbol{\mu}_1$ and $\boldsymbol{\mu}_2 = (1, 0, 0)'$ with equal volume fractions are used in R2;

- Four datasets, F1, F21, F22 and F23, are obtained with on-line DW-MR signal generator of A. Barmpoutis [1], either for a single fiber direction (F1) or for two fiber directions with equal volume fractions (F21, F22 and F23):

[1] http://www.cise.ufl.edu/ abarmpou/lab/DWMRI.simulator.php

F1	$\boldsymbol{\mu} = (\frac{\sqrt{2}}{2}, \frac{\sqrt{2}}{2}, 0)'$
F21 (90°)	$\boldsymbol{\mu}_1 = (1,0,0)'$ $\boldsymbol{\mu}_2 = (0,1,0)'$
F22 (60°)	$\boldsymbol{\mu}_1 = (1,0,0)'$ $\boldsymbol{\mu}_2 = (\frac{1}{2}, \frac{\sqrt{3}}{2}, 0)'$
F23 (45°)	$\boldsymbol{\mu}_1 = (1,0,0)'$ $\boldsymbol{\mu}_2 = (\frac{\sqrt{2}}{2}, \frac{\sqrt{2}}{2}, 0)'$

Each dataset is generated with $\phi_0 = 150$, b-value $= 1500$ s.mm^{-2} and the same set of $N = 30$ MR gradients. In addition, we generated two datasets F22/15 and F22/200 with same parameters as for F22 but with $N = 15$ and $N = 200$ MR gradients respectively.

After sampling, each dataset is corrupted by a Rician noise for 9 decreasing SNR mean values ranging from infinity (no noise) to about 3 (limiting case for which the Gaussian approximation of the Rice distribution holds). Each noisy dataset is resampled 20 times so that statistical assessment can be made on the estimated parameters.

Beside experiments on above synthetic data, we also applied DDI model on clinical data composed of $N = 30$ DW-MR images acquired with different directions and common b-value= 1000s.mm^{-2}, along with a ϕ_0 image ($b = 0$). Within these images, we selected an ROI of 12×12 voxels in the corpus callosum (Fig.3). Experiments on this data aim at showing that the use of the DDI model is appropriate for plain clinical DW-MR imaging.

3.2 Analysis of the experiments

In this section, all the statistical tests are made using the t-statistics (assuming unequal variances when two populations are compared), since Shapiro-Wilk test does not reveal any statistical evidence in favour of non-normality of the data.

In Fig. 1, we illustrate the robustness of DDI to noise. When only one fiber direction exists (left column), estimated anisotropy κ and diffusivity λ parameters are not statistically different from their respective ground truths, for all SNRs, and the angular error on the estimation of the diffusion direction does not exceed 3.5° at the lowest SNR.

When two fiber directions coexist, the same conclusions can be drawn except for the two SNRs values, lower than 3, for which Gaussian approximation of Rician noise fails to hold. The angular error on the estimated directions is overall larger when two fiber directions must be estimated. However, it does not exceed 18° at the lowest SNR while other parameters remain statistically equal to the ground truth.

In Fig. 2, we compare the ability of DDI, DTI and ODF methods to estimate fiber direction(s). Angular error is computed as the mean angular error of each estimated diffusion direction(s) with respect to its ground truth.

In presence of a single diffusion direction (graph F1 in Fig.2), the three methods seem to behave similarly, which is quantitatively confirmed by statistical tests (p-value> 0.10, for any SNR). However, when two diffusion directions

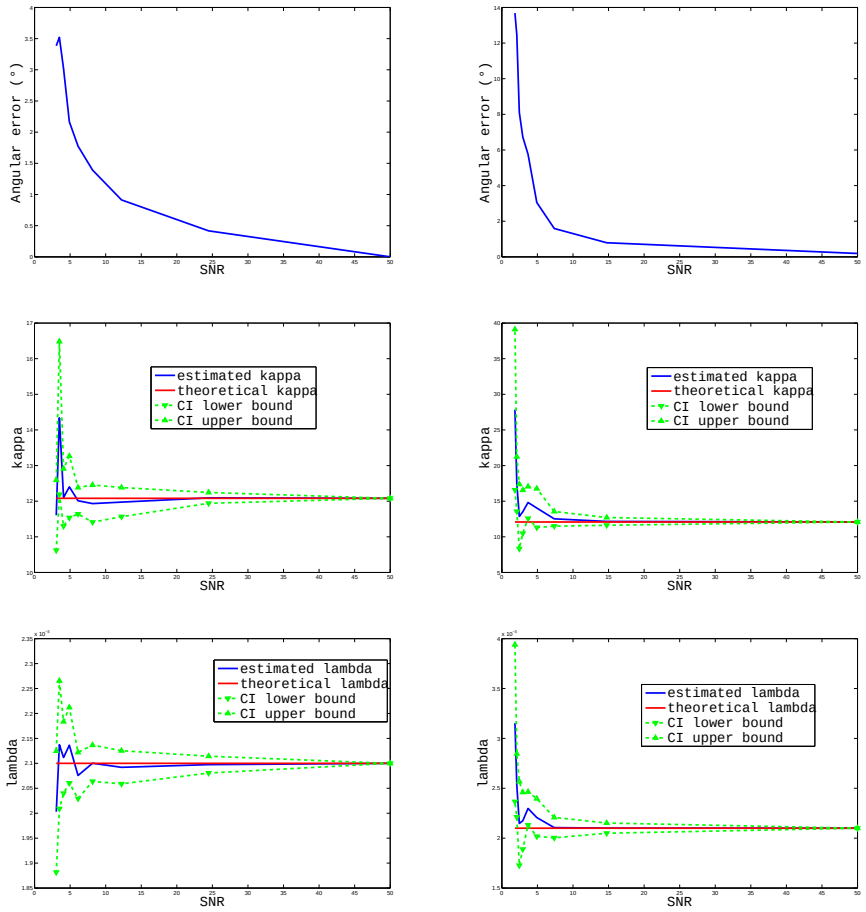

Figure 1: Noise sensitivity of DDI model when estimating: diffusion direction(s) (1st row), κ (2nd row) and λ (3rd row). Left column: R1 datasets (1 diffusion direction). Right column: R2 datasets (2 diffusion directions).

are to be estimated (other graphs in Fig.2), the angular error is most of the time lower with DDI (blue). More precisely, statistical tests allow us to conclude that

- in the situations F21 and F22 where true directions are separated by an angle of 90° and 60° respectively, DDI estimation outperforms ODF and DTI ones even for the lowest SNR (p-value< 0.05, for any SNR);
- in the situation F23 where true directions are separated by an angle of 45°, DDI estimation outperforms the others for SNR≥ 4.5 (p-value< 0.0413), but all three methods are equivalent for SNR< 4.5 (p-value> 0.05).

Also, in most situations involving two diffusion directions, DDI angular error increases linearly as the inverse of the SNR (proportional to the noise level σ) increases whereas ODF angular error seems to increase exponentially. As expected, DTI , on the other hand, seems to average the diffusion directions.

We also observe that all three methods seem to converge to an angular error around 20° as SNR goes to zero.

Finally, when the number of acquisitions varies (last row of Fig.2), ODF angular error remains fairly unaffected. DDI estimation, on the contrary, improves greatly when the number of acquisitions increases to 200 and degrades when the number of acquisitions falls to 15. Nonetheless, DDI estimation still outperforms ODF estimation with only $N = 15$ acquisitions for SNR≥ 6.5 (p-value< 0.0124).

To conclude the experimental part, we show in Fig.3 results on our real clinical data. The Fractional Anisotropy (FA) estimated by DTI is color-coded at each voxel, while arrows indicate DDI estimates (arrow direction represents estimated diffusion direction and arrow length codes estimated anisotropy). On this example, we can see that DDI model does a good job at distinguishing anisotropic regions from isotropic ones while providing a good estimation of the diffusion direction in the corpus callosum. Note that in voxel at position 2×11, both DTI and DDI estimate an unlikely anisotropy, but in a more excessive manner for DTI.

4 Discussion and Conclusion

In this paper, we proposed Diffusion Directions Imaging, a new model of diffusion for DW-MR imaging. At the heart of this model lies a careful modelling of both direction and amplitude variabilities of water molecules displacements. These three-dimensional displacements are modelled as a sum of two independent random vectors: a constant-length von Mises vector and a tri-dimensional Gaussian one. We first demonstrated that resulting model is well defined and admits a pdf. We then derived a closed-form expression linking measured DW-MR signals to DDI diffusion parameters.

Simulations on synthetic data demonstrated that diffusion directions estimated by DDI are quite robust to noise. In the worst simulated scenario (60° 2-fibers crossing) the angular error is about 18° on very noisy data (SNR= 1.84) and is about 7° on more classic data (SNR= 4). The estimation of global anisotropy and of diffusivity is also very robust to noise: the estimates of these parameters are statistically different from their ground truth only for SNR< 2.3, for the same scenarios. We remind that, for such SNR values, Gaussian approximation to the Rician noise does not hold anymore, which impairs our approximate parameter estimation.

On regions with a single fiber direction, no statistical difference has been shown between DDI, DTI and ODF estimates. As the DTI model we chose for our experiments is cylindrical-shaped, the number of its parameters turns out to be the same as for DDI model. This might explain the similar performance.

On regions with two fibers directions though, we demonstrated that DDI outperforms both DTI and ODF in the estimation of fiber directions. For all simulated types of crossing (90°, 60° and 45°), DDI estimated directions are qualitatively more accurate than DTI and ODF ones. The larger the angle separating the two diffusion directions, the more statistically significant this difference becomes on highly noisy data. Nonetheless, DDI must have an angular "resolution" of its own (shown to be smaller than the one of DTI or ODF). Crossing angles below this limit will confuse DDI estimation as well, especially in high noise regimes.

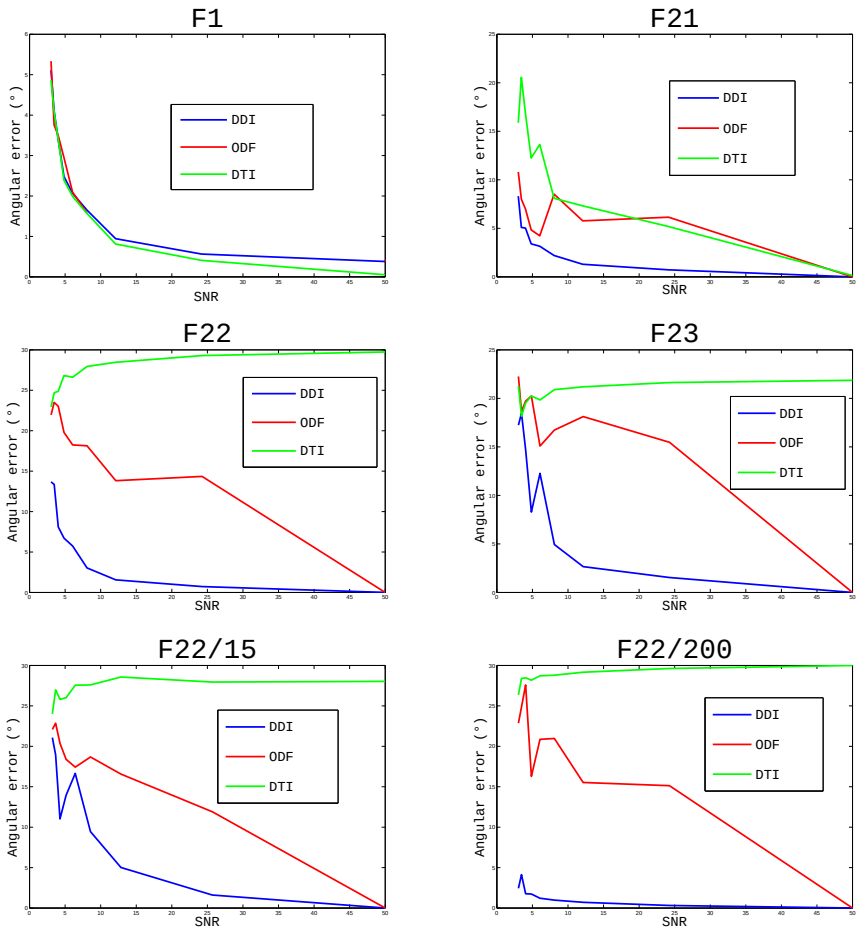

Figure 2: Comparison between DDI (blue), DTI (green) and ODF (red) regarding the precision of diffusion direction estimation: [First-second row]: for $N = 30$ acquisitions, in presence of a single direction (F1) and of a crossing of two directions with various crossing angles (F21: 90°, F22: 60°, F23: 45°); [Third row]: influence of the number of acquisitions.

Besides quantitative experiments on synthetic data, we also showed the behaviour of our approach on real clinical data when estimating fiber directions in the corpus callosum.

Most of our experiments, either on synthetic data or an clinical data, have been conducted based on a set of $N = 30$ gradient directions, which is compatible with clinical protocols. This indicates that DDI could be applied in clinical routine to get good estimates of fiber direction(s).

We dedicated this paper to the introduction of DDI model and showed its promising ability to handle multiple fiber directions, in contrast to DTI and ODF alternatives. As a perspective, we shall focus on its ability to estimate the global anisotropy and diffusivity. Related to this question, the automatic estimation of the number of directions to be estimated must be studied. Also, application

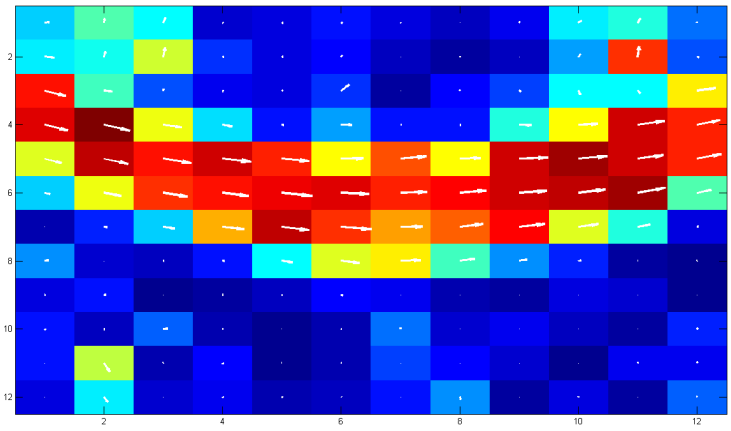

Figure 3: DDI and DTI estimates on real data within corpus callosum. Voxel color indicates fractional anisotropy estimated by DTI (red stands for high FAs). Arrows indicate the direction and the concentration of directional diffusion estimated by DDI approach.

of DDI on real clinical data with crossing or bifurcating fiber directions will be investigated.

A Some basic statistical concepts through measure theory

We can revisit many statistical tools via the measure theory. Indeed, given two measurable spaces $(E_1, \mathscr{F}_1)$ and $(E_2, \mathscr{F}_2)$, a measurable function $h : E_1 \to E_2$ and a measure $\rho : \mathscr{F}_1 \to [0, +\infty]$, we can define:

- the **pushforward measure** $h \star \rho : \mathscr{F}_2 \to [0, +\infty]$ of ρ induced by h such that $(h \star \rho)(B) = \rho\left(h^{-1}(B)\right)$, for any $B \in \mathscr{F}_2$;
- the real p-dimensional **random variable** $\mathbf{x}$ as a measurable function from the probability space $(\Omega, \mathscr{F}, P)$ to the measurable space $(\mathbb{R}^p, \mathscr{B}_p)$, where $\mathscr{B}_p$ is the Borel σ-algebra of $\mathbb{R}^p$;
- the **probability distribution** of the real p-dimensional random variable $\mathbf{x}$ as the pushforward measure of P induced by $\mathbf{x}$;
- the **characteristic function** $\varphi_{\mathbf{x}} : \mathbb{R}^p \to \mathbb{C}$ of the real p-dimensional random variable $\mathbf{x}$ such that

$$\begin{aligned}\varphi_{\mathbf{x}}(\boldsymbol{t}) &= \int_{\mathbb{R}^p} \mathrm{e}^{i\boldsymbol{t}'\boldsymbol{x}} \mathrm{d}(\mathbf{x} \star P)(\boldsymbol{x}) = \int_{\mathbb{R}^p} \mathrm{e}^{i\boldsymbol{t}'\boldsymbol{x}} \mathrm{d}P(\mathbf{x}^{-1}(\boldsymbol{x})) \\ &= \int_{\Omega} \mathrm{e}^{i\boldsymbol{t}'\mathbf{x}(\omega)} \mathrm{d}P(\omega) \ , \text{ for any } \boldsymbol{t} \in \mathbb{R}^p \ .\end{aligned}$$

- the **probability density function** $f_{\mathbf{x}} : \mathbb{R}^p \to [0, +\infty]$ of the real p-dimensional random variable $\mathbf{x}$ as the Radon-Nikodym derivative of its probability distribution.

Note that the cf of the real p-dimensional random variable $\mathbf{x}$ always exists whereas its pdf exists if and only if the probability distribution of $\mathbf{x}$ is absolutely continuous wrt the Lebesgue measure. In the latter case, the cf and the pdf are related by:

$$\varphi_{\mathbf{x}}(\boldsymbol{t}) = \int_{\mathbb{R}^p} \mathrm{e}^{i\boldsymbol{t}'\boldsymbol{x}} f_{\mathbf{x}}(\boldsymbol{x})\mathrm{d}\boldsymbol{x} \ , \text{ for any } \boldsymbol{t} \in \mathbb{R}^p \ .$$

B The von Mises & Fisher probability distribution

It is a 4-parameter probability distribution. Here is the list of the notations used throughout this section:

- $A_2 = [0,\pi] \times [0,2\pi[$ is the 2-dimensional space of spherical coordinates; equipped with its corresponding Borel σ-algebra $\mathscr{B}_{A_2}$, it is a measurable space;
- $(\theta_0, \phi_0, \kappa, R) \in A_2 \times [0,+\infty] \times]0,+\infty]$ are the parameters of the von Mises & Fisher probability distribution $F_{\theta_0,\phi_0,\kappa,R}$;
- $\boldsymbol{\mu} = (\sin\theta_0\cos\phi_0, \sin\theta_0\sin\phi_0, \cos\theta_0)'$ and the von Mises & Fisher distribution can also be denoted by $F_{\boldsymbol{\mu},\kappa,R}$;
- $\nu_{\boldsymbol{\mu},\kappa} : \mathscr{B}_{A_2} \to [0,+\infty]$ is the measure whose density wrt the Lebesgue measure reads:

$$\begin{aligned}\mathrm{d}\nu_{\boldsymbol{\mu},\kappa}(\theta,\phi) = \frac{\kappa\sin\theta}{4\pi\mathrm{sh}\,\kappa} \exp\{\kappa(\mu_1\sin\theta\cos\phi \\ +\mu_2\sin\theta\sin\phi + \mu_3\cos\theta)\}\,\mathrm{d}\theta\mathrm{d}\phi \ ,\end{aligned} \tag{11}$$

for any $(\theta,\phi) \in A_2$ so that $(A_2, \mathscr{B}_{A_2}, \nu_{\boldsymbol{\mu},\kappa})$ is a probability space;

- T_R is the real 3-dimensional random variable from $(A_2, \mathscr{B}_{A_2}, \nu_{\boldsymbol{\mu},\kappa})$ to $\left(\mathbb{R}^3, \mathscr{B}_3\right)$ such that

$$T_R(\theta,\phi) = (R\sin\theta\cos\phi, R\sin\theta\sin\phi, R\cos\theta)' \ , \tag{12}$$

for any $(\theta,\phi) \in A_2$.

Definition: The von Mises & Fisher probability distribution is the push-forward measure $F_{\boldsymbol{\mu},\kappa,R}$ of $\nu_{\boldsymbol{\mu},\kappa}$ induced by T_R: $\boldsymbol{\mu}$ (unit vector) is the *mean direction*, $\kappa \geq 0$ is the *concentration parameter* which evaluates the dispersion of the probability distribution around the mean direction $\boldsymbol{\mu}$ and $R > 0$ is the radius of the sphere on which the probability distribution has positive value.

Characteristic function: Let $\mathbf{u}$ be a real 3-dimensional random variable following the von Mises & Fisher probability distribution $F_{\boldsymbol{\mu},\kappa,R}$. Then, for any $\boldsymbol{t} \in \mathbb{R}^3$, its characteristic function is

$$\varphi_{\mathbf{u}}(\boldsymbol{t};\boldsymbol{\mu},\kappa,R) = \int_{A^2} \mathrm{e}^{i\boldsymbol{t}'T_R(\theta,\phi)}\mathrm{d}\nu_{\boldsymbol{\mu},\kappa}(\theta,\phi) \ .$$

which, combined with Eq.(11), becomes

$$\varphi_{\mathbf{u}}(\boldsymbol{t};\boldsymbol{\mu},\kappa,R) = \frac{\kappa}{4\pi\mathrm{sh}\,\kappa} \int_{A^2} \mathrm{e}^{(iR\boldsymbol{t}+\kappa\boldsymbol{\mu})'T_1(\theta,\phi)} \sin\theta\mathrm{d}\theta\mathrm{d}\phi \ .$$

The derivation of this integral is carried out in [57] for the case $R = 1$. It is straightforward to generalize the expression for any $R > 0$:

$$\varphi_{\mathbf{u}}(\boldsymbol{t};\boldsymbol{\mu},\kappa,R) = \frac{\kappa}{\mathrm{sh}\,\kappa} \sum_{n=0}^{+\infty} \frac{z^n}{(2n+1)!} \ , \forall \boldsymbol{t} \in \mathbb{R}^3 \ ,$$

with $z = z(\boldsymbol{t};\boldsymbol{\mu},\kappa,R) = \kappa^2 - R^2\|\boldsymbol{t}\|^2 + 2i\kappa R\boldsymbol{\mu}'\boldsymbol{t}$.
This expression can be simplified by introducing:

$$\begin{aligned}\alpha = \alpha(\boldsymbol{t};\boldsymbol{\mu},\kappa,R) &= \sqrt{\frac{\mathrm{Re}\ z + |z|}{2}}\ , \text{ and }\ ,\\ \beta = \beta(\boldsymbol{t};\boldsymbol{\mu},\kappa,R) &= \frac{\mathrm{Im}\ z}{\sqrt{2\,(\mathrm{Re}\ z + |z|)}}\ ,\end{aligned} \tag{13}$$

provided that these quantities are well-defined ($\mathrm{Re}\ z + |z| > 0$), which leads to:

$$\varphi_{\mathbf{u}}(\boldsymbol{t};\boldsymbol{\mu},\kappa,R) = \begin{cases} \dfrac{\kappa}{\mathrm{sh}\,\kappa}\dfrac{\sin\sqrt{R^2\|\boldsymbol{t}\|^2 - \kappa^2}}{\sqrt{R^2\|\boldsymbol{t}\|^2 - \kappa^2}}\ ,\ \boldsymbol{t}\in\Omega\ ,\\ \dfrac{\kappa}{\mathrm{sh}\,\kappa}\dfrac{\mathrm{sh}\,(\alpha+i\beta)}{\alpha+i\beta}\ ,\ \boldsymbol{t}\notin\Omega\ ,\end{cases} \tag{14}$$

where $\Omega = \left\{\boldsymbol{t}\in\mathbb{R}^3 \text{ s.t. } \|\boldsymbol{t}\| \geq \kappa/R \ \&\ \boldsymbol{t}\perp\boldsymbol{\mu}\right\}$ if $\kappa > 0$ or $\Omega = \mathbb{R}^3$ if $\kappa = 0$.

Remarks. When $\kappa = 0$, the von Mises & Fisher probability distribution coincides with the uniform probability distribution on the 2-dimensional sphere of radius R.
Besides, the von Mises & Fisher probability distribution is not absolutely continuous wrt the Lebesgue measure in $\mathbb{R}^3$ as, for example, A_2 has null Lebesgue measure while $F_{\boldsymbol{\mu},\kappa,R}(A_2) = 1$. Therefore, it does not admit a pdf on $\mathbb{R}^3$.

C Independent sum of a von Mises & Fisher variable and a Gaussian variable

Let $\mathbf{w}$ be the independent sum of a von Mises & Fisher random variable $\mathbf{u}$ defined on the 2-dimensional sphere of radius $R > 0$ with pdf given by Eq.(2) and a Gaussian random variable $\mathbf{v}$ defined on $\mathbb{R}^3$ with pdf given by Eq.(3). The random variable $\mathbf{w}$ admits both a cf and a pdf. For any $\boldsymbol{t}\in\mathbb{R}^3$, the former is given by:

$$\varphi_{\mathbf{w}}(\boldsymbol{t};\boldsymbol{\mu},\kappa,R) = \varphi_{\mathbf{u}}(\boldsymbol{t};\boldsymbol{\mu},\kappa,R)\varphi_{\mathbf{v}}(\boldsymbol{t};\boldsymbol{\mu},\kappa,R)\ ,$$

where $\varphi_{\mathbf{u}}(\boldsymbol{t};\boldsymbol{\mu},\kappa,R)$ is given by Eq.(14) and

$$\varphi_{\mathbf{v}}(\boldsymbol{t};\boldsymbol{\mu},\kappa,R) = \mathrm{e}^{-\frac{R^2}{2(\kappa+1)}\left(\|\boldsymbol{t}\|^2+\kappa(\boldsymbol{\mu}'\boldsymbol{t})^2\right)}\ ,$$

and, for any $\boldsymbol{w}\in\mathbb{R}^3$, the latter is given by:

$$\begin{aligned}f_{\mathbf{w}}(\boldsymbol{w};\boldsymbol{\mu},\kappa,R) &= c(\kappa,R)\mathrm{e}^{-\frac{1}{2}\left((\kappa+1)w_\perp^2+w_{/\!/}^2\right)}\\ &\times\int_{-1}^{1}\mathrm{e}^{\frac{\kappa}{2}t^2+(\kappa+w_{/\!/})t}I_0\left((\kappa+1)w_\perp\sqrt{1-t^2}\right)dt\ ,\end{aligned}$$

where (i) $(w_{/\!/},w_\perp) := R^{-1}\left(\boldsymbol{\mu}'\boldsymbol{w},\sqrt{\|\boldsymbol{w}\|^2-(\boldsymbol{\mu}'\boldsymbol{w})^2}\right)$,
(ii) $c(\kappa,R) := \dfrac{\kappa(\kappa+1)\sqrt{2}}{8\pi^{3/2}R^3\mathrm{sh}\,(\kappa)}\mathrm{e}^{-\frac{\kappa+1}{2}}$ and (iii) I_0 is the zero-*th* order modified Bessel function [48], with the convention that $\boldsymbol{\mu}'\boldsymbol{w} = \|\boldsymbol{w}\|$ for any $\boldsymbol{w}\in\mathbb{R}^3$ when $\kappa = 0$.

Proof:

Let $F_{\boldsymbol{\mu},\kappa,R}$, $G_{\boldsymbol{\mu},\kappa,R}$ and $H_{\boldsymbol{\mu},\kappa,R}$ be the probability distributions of the real 3-dimensional random variables $\mathbf{u}$, $\mathbf{v}$ and $\mathbf{w}$ respectively. The statistical independence of the random variables $\mathbf{u}$ and $\mathbf{v}$ implies that:

- the characteristic function of $\mathbf{w}$ reads $\varphi_{\mathbf{w}} = \varphi_{\mathbf{u}+\mathbf{v}} = \varphi_{\mathbf{u}}\varphi_{\mathbf{v}}$; using the expression of the cf of the Gaussian random variable [58] ends the proof for $\varphi_{\mathbf{w}}$;
- the density of $H_{\boldsymbol{\mu},\kappa,R}$ wrt $G_{\boldsymbol{\mu},\kappa,R}$ reads

$$\mathrm{d}H_{\boldsymbol{\mu},\kappa,R}(\boldsymbol{w}) = \int_{\mathbb{R}^3} \mathrm{d}G_{\boldsymbol{\mu},\kappa,R}(\boldsymbol{w}-\boldsymbol{u})\mathrm{d}F_{\boldsymbol{\mu},\kappa,R}(\boldsymbol{u}) \ ,$$

for any $\boldsymbol{w} \in \mathbb{R}^3$; now, $G_{\boldsymbol{\mu},\kappa,R}$ is absolutely continuous wrt the Lebesgue measure, so does $H_{\boldsymbol{\mu},\kappa,R}$. The pdf of $\mathbf{w}$ thereby exists and is given, for any $\boldsymbol{w} \in \mathbb{R}^3$, by

$$f_{\mathbf{w}}(\boldsymbol{w};\boldsymbol{\mu},\kappa,R) = \int_{\mathbb{R}^3} f_{\mathbf{v}}(\boldsymbol{w}-\boldsymbol{u};\boldsymbol{\mu},\kappa,R)\mathrm{d}F_{\boldsymbol{\mu},\kappa,R}(\boldsymbol{u}) \ .$$

Since $F_{\boldsymbol{\mu},\kappa,R}$ is a von Mises & Fisher probability distribution, it is the push-forward measure of $\nu_{\boldsymbol{\mu},\kappa}$ defined in Eq.(11) induced by the random variable T_R defined in Eq.(12). We thus have:

$$\mathrm{d}F_{\boldsymbol{\mu},\kappa,R}(\boldsymbol{u}) = \mathrm{d}\nu_{\boldsymbol{\mu},\kappa}\left(T_R^{-1}(\boldsymbol{u})\right) \ , \forall \boldsymbol{u} \in \mathbb{R}^3 \ . \tag{15}$$

Combining Eq.(3), Eq.(11) and Eq.(15), we obtain after some simplifications:

$$\begin{aligned} f_{\mathbf{w}}(\boldsymbol{w};\boldsymbol{\mu},\kappa,R) = \frac{c(\kappa,R)}{2\pi}\mathrm{e}^{-\frac{1}{2}\left((\kappa+1)w_\perp + w_{/\!/}\right)} \\ \times Q(\boldsymbol{w};\boldsymbol{\mu},\kappa,R) \ , \end{aligned} \tag{16}$$

where $Q : \mathbb{R}^3 \to \mathbb{R}$ is defined as follows:

$$\begin{aligned} Q(\boldsymbol{w};\boldsymbol{\mu},\kappa,R) := \int_{A_2} \mathrm{e}^{\frac{\kappa}{2}\left(\boldsymbol{\mu}' T_1(\theta,\phi)\right)^2} \mathrm{e}^{\kappa\left(1-\frac{\boldsymbol{\mu}'\boldsymbol{w}}{R}\right)\boldsymbol{\mu}' T_1(\theta,\phi)} \\ \times \mathrm{e}^{\frac{\kappa+1}{R}\boldsymbol{w}' T_1(\theta,\phi)} \sin\theta \mathrm{d}\theta\mathrm{d}\phi \ . \end{aligned}$$

The expression of Q, which involves a double integral, can be simplified by means of Bessel functions [48] to obtain a single-integral formulation:

$$\begin{aligned} Q(\boldsymbol{w};\boldsymbol{\mu},\kappa,R) = 2\pi \int_{-1}^{1} \mathrm{e}^{\frac{\kappa}{2}t^2 + \left(\kappa + w_{/\!/}\right)t} \\ \times I_0\left((\kappa+1)w_\perp\sqrt{1-t^2}\right) dt \ . \end{aligned} \tag{17}$$

The details of its derivation are quite technical and available upon request of the reader. We choose not to report them here as they are not essential for the scope of this work.

Inserting Eq.(17) into Eq.(16) ends the proof for $f_{\mathbf{x}}$.

References

[1] D. Le Bihan, "Looking into the functional architecture of the brain with diffusion MRI." *Nature reviews. Neuroscience*, vol. 4, no. 6, pp. 469–80, 2003.

[2] P. T. Callaghan, C. D. Eccles, and Y. Xia, "Nmr microscopy of dynamic displacements: k-space and q-space imaging," *Journal of Physics E: Scientific Instruments*, vol. 21, no. 8, p. 820, 1988.

[3] D. C. Alexander, *An introduction to computational diffusion MRI: the diffusion tensor and beyond*, ser. Visualization and Processing of Tensor Fields. Springer Berlin Heidelberg, 2006, ch. 5, pp. 83–106.

[4] H. Gudbjartsson and S. Patz, "The Rician distribution of noisy MRI data," *Magnetic Resonance in Medicine*, vol. 34, no. 6, pp. 910–914, 1995.

[5] C. Constantinides, E. Atalar, and M. ER, "Signal-to-noise measurements in magnitude images from NMR phased arrays," *Magnetic resonance in medicine : official journal of the Society of Magnetic Resonance in Medicine / Society of Magnetic Resonance in Medicine*, vol. 38, no. 5, pp. 852–857, 1997.

[6] E. O. Stejskal, "Use of Spin Echoes in a Pulsed Magnetic-Field Gradient to Study Anisotropic, Restricted Diffusion and Flow," *The Journal of Chemical Physics*, vol. 43, no. 10, pp. 3597–3603, 1965.

[7] P. T. Callaghan, *Principles of Nuclear Magnetic Resonance Microscopy*. Oxford University Press, 1991.

[8] H.-E. Assemlal, D. Tschumperlé, L. Brun, and K. Siddiqi, "Recent advances in diffusion MRI modeling: Angular and radial reconstruction." *Medical image analysis*, 2011.

[9] V. Wedeen, T. Reese, D. Tuch, M. Weigel, J. Dou, R. Weiskoff, and D. Chessler, "Mapping fiber orientation spectra in cerebral white matter with Fourier-transform diffusion MRI," in *Proc. Intl. Sot. Mag. Reson. Med*, vol. 8, 2000, p. 82.

[10] D. Tuch, "Diffusion MRI of complex tissue structure," Ph.D. dissertation, 2002.

[11] V. J. Wedeen, R. P. Wang, J. D. Schmahmann, T. Benner, W. Y. I. Tseng, G. Dai, D. N. Pandya, P. Hagmann, H. D'Arceuil, and a. J. de Crespigny, "Diffusion spectrum magnetic resonance imaging (DSI) tractography of crossing fibers." *NeuroImage*, vol. 41, no. 4, pp. 1267–77, 2008.

[12] Y. Wu and A. Alexander, "Hybrid diffusion imaging," *NeuroImage*, vol. 36, no. 3, pp. 617–629, 2007.

[13] A. Barmpoutis, B. Vemuri, and J. Forder, "Fast displacement probability profile approximation from hardi using 4th-order tensors," in *Biomedical Imaging: From Nano to Macro, 2008. ISBI 2008. 5th IEEE International Symposium on.* IEEE, 2008, pp. 911–914.

[14] A. Ghosh and R. Deriche, "Fast and closed-form ensemble-average-propagator approximation from the 4th-order diffusion tensor," in *Biomedical Imaging: From Nano to Macro, 2010 IEEE International Symposium on.* IEEE, 2010, pp. 1105–1108.

[15] H.-E. Assemlal, D. Tschumperlé, and L. Brun, "Efficient and robust computation of PDF features from diffusion MR signal." *Medical image analysis*, vol. 13, no. 5, pp. 715–29, 2009.

[16] J. Cheng, A. Ghosh, T. Jiang, and R. Deriche, "Model-free and analytical EAP reconstruction via spherical polar Fourier diffusion MRI." *Medical image computing and computer-assisted intervention : MICCAI ... International Conference on Medical Image Computing and Computer-Assisted Intervention*, vol. 13, no. Pt 1, pp. 590–7, 2010.

[17] M. Descoteaux, R. Deriche, D. Le Bihan, J.-F. Mangin, and C. Poupon, "Multiple q-shell diffusion propagator imaging." *Medical image analysis*, pp. 1–19, 2010.

[18] C. Liu, R. Bammer, B. Acar, and M. E. Moseley, "Characterizing non-Gaussian diffusion by using generalized diffusion tensors." *Magnetic resonance in medicine : official journal of the Society of Magnetic Resonance in Medicine / Society of Magnetic Resonance in Medicine*, vol. 51, no. 5, pp. 924–37, 2004.

[19] D. S. Tuch, T. G. Reese, M. R. Wiegell, N. Makris, J. W. Belliveau, and V. J. Wedeen, "High Angular Resolution Diffusion Imaging reveals intravoxel white matter fiber heterogeneity," *Magnetic Resonance in Medicine*, vol. 48, pp. 577–582, 2002.

[20] J. G. Malcolm, O. Michailovich, S. Bouix, C.-F. Westin, M. E. Shenton, and Y. Rathi, "A filtered approach to neural tractography using the Watson directional function," *Medical Image Analysis*, vol. 14, no. 1, pp. 58 – 69, 2010.

[21] T. E. J. Behrens, M. W. Woolrich, M. Jenkinson, H. Johansen-Berg, R. G. Nunes, S. Clare, P. M. Matthews, J. M. Brady, and S. M. Smith, "Characterization and propagation of uncertainty in diffusion-weighted MR imaging." *Magn. Res. Med.*, vol. 50, no. 5, pp. 1077–88, Nov. 2003.

[22] B. Scherrer and S. K. Warfield, "Why multiple b-values are required for multi-tensor models. Evaluation with a constrained log-euclidean model," in *IEEE ISBI'10*, 2010, pp. 1389–1392.

[23] D. Tuch, R. Weisskoff, J. Belliveau, and V. Wedeen, "High angular resolution diffusion imaging of the human brain," in *Proceedings of the 7th Annual Meeting of ISMRM*, 1999, p. 321.

[24] D. S. Tuch, "Q-ball imaging." *Magnetic resonance in medicine : official journal of the Society of Magnetic Resonance in Medicine / Society of Magnetic Resonance in Medicine*, vol. 52, no. 6, pp. 1358–72, 2004.

[25] E. Ozarslan, T. M. Shepherd, B. C. Vemuri, S. J. Blackband, and T. H. Mareci, "Resolution of complex tissue microarchitecture using the diffusion orientation transform (DOT)." *NeuroImage*, vol. 31, no. 3, pp. 1086–103, 2006.

[26] I. Aganj, C. Lenglet, G. Sapiro, E. Yacoub, K. Ugurbil, and N. Harel, "Reconstruction of the orientation distribution function in single- and multiple-shell q-ball imaging within constant solid angle." *Magnetic resonance in medicine : official journal of the Society of Magnetic Resonance in Medicine / Society of Magnetic Resonance in Medicine*, vol. 64, no. 2, pp. 554–66, 2010.

[27] A. W. Anderson, "Measurement of fiber orientation distributions using high angular resolution diffusion imaging." *Magnetic resonance in medicine : official journal of the Society of Magnetic Resonance in Medicine / Society of Magnetic Resonance in Medicine*, vol. 54, no. 5, pp. 1194–206, 2005.

[28] C. P. Hess, P. Mukherjee, E. T. Han, D. Xu, and D. B. Vigneron, "Q-ball reconstruction of multimodal fiber orientations using the spherical harmonic basis." *Magnetic resonance in medicine : official journal of the Society of Magnetic Resonance in Medicine / Society of Magnetic Resonance in Medicine*, vol. 56, no. 1, pp. 104–17, 2006.

[29] M. Descoteaux, E. Angelino, S. Fitzgibbons, and R. Deriche, "Regularized, Fast, and Robust Analytical Q-Ball Imaging," *Magn Res Med*, vol. 58, pp. 497–510, 2007.

[30] Y. Assaf, R. Z. Freidlin, G. K. Rohde, and P. J. Basser, "New modeling and experimental framework to characterize hindered and restricted water diffusion in brain white matter." *Magnetic resonance in medicine : official journal of the Society of Magnetic Resonance in Medicine / Society of Magnetic Resonance in Medicine*, vol. 52, no. 5, pp. 965–78, 2004.

[31] C. Neuman, "Spin echo of spins diffusing in a bounded medium," *Journal of Chemical Physics*, vol. 60, no. 11, pp. 4508–11, 1974.

[32] D. Healy, "Spherical Deconvolution," *Journal of Multivariate Analysis*, vol. 67, no. 1, pp. 1–22, 1998.

[33] B. Jian and B. Vemuri, "A unified computational framework for deconvolution to reconstruct multiple fibers from diffusion weighted MRI," *Medical Imaging, IEEE Transactions on*, vol. 26, no. 11, pp. 1464–1471, 2007.

[34] A. Anderson and Z. Ding, "Sub-voxel measurement of fiber orientation using high angular resolution diffusion tensor imaging," in *Book of abstracts: Tenth Annual Meeting of the International Society for Magnetic Resonance in Medicine. Berkeley, CA: ISMRM*, vol. 10, 2002, p. 440.

[35] M. Descoteaux, R. Deriche, T. R. Knösche, and A. Anwander, "Deterministic and probabilistic tractography based on complex fibre orientation distributions." *IEEE transactions on medical imaging*, vol. 28, no. 2, pp. 269–86, 2009.

[36] B. Jian, B. Vemuri, E. Ozarslan, P. Carney, and T. Mareci, "A novel tensor distribution model for the diffusion-weighted MR signal," *NeuroImage*, vol. 37, no. 1, pp. 164–176, 2007.

[37] D. Alexander, "Maximum entropy spherical deconvolution for diffusion MRI," in *Information Processing in Medical Imaging*. Springer, 2005, pp. 76–87.

[38] K. Jansons and D. Alexander, "Persistent angular structure: new insights from diffusion magnetic resonance imaging data," *Inverse problems*, vol. 19, p. 1031, 2003.

[39] J.-D. Tournier, F. Calamante, D. G. Gadian, and A. Connelly, "Direct estimation of the fiber orientation density function from diffusion-weighted MRI data using spherical deconvolution." *NeuroImage*, vol. 23, no. 3, pp. 1176–85, 2004.

[40] E. Kaden, T. R. Knï¿½sche, and A. Anwander, "Parametric spherical deconvolution: Inferring anatomical connectivity using diffusion MR imaging," *NeuroImage*, vol. 37, no. 2, pp. 474 – 488, 2007.

[41] A. Barmpoutis, B. Jian, and B. C. Vemuri, "Adaptive kernels for multi-fiber reconstruction." *IPMI*, vol. 21, pp. 338–49, Jan. 2009.

[42] P. J. Basser, J. Mattiello, and D. LeBihan, "MR diffusion tensor spectroscopy and imaging." *Biophysical journal*, vol. 66, no. 1, pp. 259–67, 1994.

[43] S. Merlet and R. Deriche, "Compressed Sensing for Accelerated EAP Recovery in Diffusion MRI," in *MICCAI*, 2010, p. Page 14.

[44] S. Merlet, J. Cheng, A. Ghosh, and R. Deriche, "Spherical Polar Fourier EAP and ODF Reconstruction via Compressed Sensing in Diffusion MRI," in *ISBI*, 2011.

[45] P. Jupp and K. Mardia, "A unified view of the theory of directional statistics, 1975-1988," *International Statistical Review*, vol. 57, no. 3, pp. 261–294, 1989.

[46] O. Friman and C.-F. Westin, "Uncertainty in white matter fiber tractography." *International Conference on Medical Image Computing and Computer-Assisted Intervention*, vol. 8, no. 1, pp. 107–14, 2005.

[47] W. Hager, "Updating the inverse of a matrix," *SIAM review*, vol. 31, no. 2, pp. 221–239, 1989.

[48] M. Abramowitz and I. A. Stegun, *Handbook of mathematical functions with formulas, graphs and mathematical tables*, 9th ed. Dover Publications, 1972.

[49] P. J. Basser and C. Pierpaoli, "Microstructural and physiological features of tissues elucidated by quantitative diffusion tensor MRI," *J Magn Res*, vol. 111, no. 86, pp. 209–219, 1996.

[50] S. Peled, O. Friman, F. Jolesz, and C.-F. Westin, "Geometrically constrained two-tensor model for crossing tracts in DWI," *Magn. Res. Imag.*, vol. 24, no. 9, pp. 1263–1270, 2006.

[51] E. O. Stejskal and J. E. Tanner, "Spin Diffusion Measurements: Spin Echoes in the Presence of a Time-Dependent Field Gradient," *The Journal of Chemical Physics*, vol. 42, no. 1, p. 288, 1965.

[52] P. J. Basser, "Relationships between diffusion tensor and q-space MRI." *Magnetic resonance in medicine : official journal of the Society of Magnetic Resonance in Medicine / Society of Magnetic Resonance in Medicine*, vol. 47, no. 2, pp. 392–7, 2002.

[53] R. Henkelman, "Measurement of signal intensities in the presence of noise in MR images," *Medical Physics*, vol. 12, no. 2, pp. 232–233, 1985.

[54] S. Aja-Fernández, M. Niethammer, M. Kubicki, M. Shenton, and C. Westin, "Restoration of DWI data using a Rician LMMSE estimator," *Trans. Med. Imaging*, vol. 27, no. 10, pp. 1389–1403, 2008.

[55] M. Powell, "The NEWUOA software for unconstrained optimization without derivatives," in *Large-Scale Nonlinear Optimization*, ser. Nonconvex Optimization and Its Applications, P. Pardalos, G. Pillo, and M. Roma, Eds. Springer US, 2006, vol. 83, pp. 255–297.

[56] K. Burnham and D. Anderson, *Model Selection and Multimodel Inference: A Practical Information-Theoretic Approach*. Springer-Verlag, 2002.

[57] S. Dégerine, "Lois de von Mises et lois liÃ©es," *Annales de l'Institut Henri PoincarÃ©*, vol. 15, no. 1, pp. 63–77, 1979.

[58] T. Anderson, *An introduction to multivariate statistical analysis*, ser. Wiley series in probability and mathematical statistics. Probability and mathematical statistics. Wiley-Interscience, 2003.

Centre de recherche INRIA Rennes – Bretagne Atlantique
IRISA, Campus universitaire de Beaulieu - 35042 Rennes Cedex (France)

Centre de recherche INRIA Bordeaux – Sud Ouest : Domaine Universitaire - 351, cours de la Libération - 33405 Talence Cedex
Centre de recherche INRIA Grenoble – Rhône-Alpes : 655, avenue de l'Europe - 38334 Montbonnot Saint-Ismier
Centre de recherche INRIA Lille – Nord Europe : Parc Scientifique de la Haute Borne - 40, avenue Halley - 59650 Villeneuve d'Ascq
Centre de recherche INRIA Nancy – Grand Est : LORIA, Technopôle de Nancy-Brabois - Campus scientifique
615, rue du Jardin Botanique - BP 101 - 54602 Villers-lès-Nancy Cedex
Centre de recherche INRIA Paris – Rocquencourt : Domaine de Voluceau - Rocquencourt - BP 105 - 78153 Le Chesnay Cedex
Centre de recherche INRIA Saclay – Île-de-France : Parc Orsay Université - ZAC des Vignes : 4, rue Jacques Monod - 91893 Orsay Cedex
Centre de recherche INRIA Sophia Antipolis – Méditerranée : 2004, route des Lucioles - BP 93 - 06902 Sophia Antipolis Cedex

Éditeur
INRIA - Domaine de Voluceau - Rocquencourt, BP 105 - 78153 Le Chesnay Cedex (France)
http://www.inria.fr
ISSN 0249-6399